Shape-Selective Catalysis

Deutsche Ausgabe: DOI: 10.1002/ange.201602429
Internationale Ausgabe: DOI: 10.1002/anie.201602429

Encapsulating Palladium Nanoparticles Inside Mesoporous MFI Zeolite Nanocrystals for Shape-Selective Catalysis

Tian-Lu Cui, Wen-Yu Ke, Wen-Bei Zhang, Hong-Hui Wang, Xin-Hao Li, and Jie-Sheng Chen**

Abstract: *Pd nanoparticles were successfully encapsulated inside mesoporous silicalite-1 nanocrystals (Pd@mnc-S1) by a one-pot method. The as-synthesized Pd@mnc-S1 with excellent stability functioned as an active and reusable heterogeneous catalyst. The unique porosity and nanostructure of silicalite-1 crystals endowed the Pd@mnc-S1 material general shape-selectivity for various catalytic reactions, including selective hydrogenation, oxidation, and carbon–carbon coupling reactions.*

Catalysts based on metal nanoparticles having excellent catalytic properties suggest numerous applications,[1] which however usually suffer from particle aggregation at high temperature and/or during the reaction process and thus a corresponding loss of catalytic activity. Much effort has been devoted to resolving the stability issue of nanoparticle-based catalysts.[2] Generally, nanoparticles were dispersed onto/into the solid supports to impede the sintering of nanoparticles under high-temperature environments.[3] Considering the diffusion limitation of bulk derivatives, mesoscale catalyst supports with high surface area were usually preferred for practical uses.[4] Typically, micrometer-sized particles or nanoparticles with short, unhindered mesochannels and thus favorable mass-transfer efficiency are beneficial for catalysis. Therefore, engineering porous materials into nanostructures has attracted much attention as catalyst supports for stabilizing specific active nanoparticles.

Besides stability and mass-transfer efficiency originating from textural features of nanostructured porous catalyst supports, on-demand control in the selectivity of metal nanoparticle-based catalysts should be the third aspect to be considered for the design of highly efficient heterogeneous catalysts. Current approaches to modifying the reaction selectivity of supported metal nanoparticles were mainly focused on surface coating by using organic ligands or amorphous metal oxides as added layers.[5] Principally, merging the shape-selectivity of zeolites with the high activity of metal nanocatalysts may lead to controllable selectivity of their hybrids.[6] As a result, integrating metal nanoparticles inside zeolite crystals is the key point to ensure the successful merging of the advantages of these two components, and is also highly challenging for material synthesis.

Moreover, the small size of micropores of most zeolites tends to hinder the diffusion rate of reactants and more or less limits their performance in catalysis.[6,7] Again, rationally balancing the shape selectivity of micropores and mass diffusion efficiencies of zeolite supports should be another great challenge for further improving the catalytic performance of metal nanoparticle/zeolite hybrids. A powerful synthesis therefore includes the completely encapsulating metal nanoparticles inside zeolite crystals and rational control of the mesopores and/or small size of these zeolite crystals simultaneously.

Herein, we report a one-pot method for the facile synthesis of Pd nanoparticle/ silicalite-1 nanocrystal hybrids (Pd@mnc-S1) with Pd nanoparticles encapsulated inside the mesoporous silicalite-1 nanocrystals. The highly integrated structure of Pd@mnc-S1 ensured the high thermal stability and also chemical stability of Pd nanoparticles. The intrinsic micropores of silicalite-1 endowed general shape selectivity of Pd nanoparticles for a series of model reactions, including hydrogenation, oxidation and C–C coupling reactions. The introduction of mesopores as well as the nanostructures of zeolite supports ensured the mass-transfer efficiency and thus high catalytic activity for practical uses.

As shown in Scheme 1, a simple one-pot method was applied to the synthesis of Pd@mnc-S1 from silica nanoparticles and chloropalladic acid. A modified Kirkendall growth process, the mechanism of which has been well-investigated in our previous work,[8] was well-controlled here to ensure the complete integration of Pd nanoparticles inside mesoporous silicalite-1 nanocrystals rather than on their surface. A small amount of polyvinyl pyrrolidone (PVP, K30) was also added to the mixed dispersion of silica nanoparticles and chloropalladic acid to keep the as-formed palladium oxide or hydroxide nanoparticles (Supporting Information, Figure S1) from aggregation during the process of tuning the pH value of the mixture to 12. Further removal of solvent from the mixed dispersion resulted in amorphous silica aerogel (Supporting Information, Figure S1). The aerogel was further moved to an autoclave and heated at 120 °C in the

[*] T. L. Cui, W. Y. Ke, W. B. Zhang, H. H. Wang, Prof. Dr. X. H. Li, Prof. Dr. J. S. Chen
School of Chemistry and Chemical Engineering
Shanghai Jiao Tong University
Shanghai 200240 (P. R. China)
E-mail: xinhaoli@sjtu.edu.cn
chemcj@sjtu.edu.cn

Supporting information for this article can be found under: http://dx.doi.org/10.1002/anie.201602429.

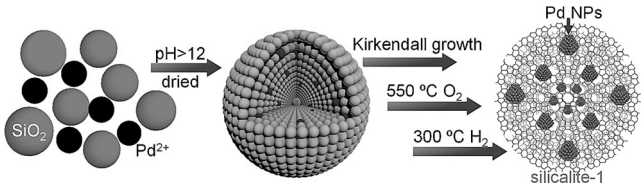

Scheme 1. The proposed synthesis processes of Pd@mnc-S1.

 © 2016 Wiley-VCH Verlag GmbH & Co. KGaA, Weinheim

presence of a limited amount of water to trigger the Kirkendall growth of silicalite-1 nanocrystals with built-in mesopores. Successive calcination of the as-obtained solid after the Kirkendall growth process in oxygen and hydrogen atmospheres were conducted to remove all possible organic components and reduce palladium oxide nanoparticles to metallic ones, respectively.

Basic characterizations were conducted to survey the textural properties of Pd@mnc-S1. The involvement of Pd nanoparticles did not disturb the mesoporous structure and crystallinity of the host silicalite-1 nanocrystals. Large-area transmission electron microscopy (TEM; Supporting Information, Figure S2) and scanning electron microscope (SEM) images (Supporting Information, Figure S3) demonstrated the formation of silicalite-1 nanoparticles with a mean size around 200 nm. The high-resolution TEM (HRTEM, Figure 1 a) image of a typical Pd@mnc-S1 nanoparticle with clearly distinguishable and oriented lattice fringes of MFI zeolite revealed the high crystallinity of the whole silicalite-1 nanocrystal, which was further demonstrated by the X-ray diffraction (XRD) pattern (Supporting Information, Figure S4). The formation of metallic Pd nanoparticles was well confirmed by the XRD (Supporting Information, Figure S4) and the energy-dispersive spectroscopy (EDS) results (Supporting Information, Figure S5). The weight percentage of Pd nanoparticles was estimated to be 1.7 wt % according to the X-ray fluorescence spectrometer (XRF) analysis (data not shown). Corresponding elemental mapping images (Supporting Information, Figure S6) further indicated the homogeneous distribution of Pd nanoparticles in the silicalite-1 nanocrystals.

The porous structure of Pd@mnc-S1 was directly reflected by brighter areas in the HRTEM image of silicalite-1 nanocrystals (Figure 1 a). The N_2 adsorption/desorption isotherm (Figure 1 b) exhibited a steep increase at relative pressure $P/P_0 < 0.02$, signifying the presence of microporosity with a Horvath–Kawazoe (HK, Figure 1 c left) pore size distribution centered at 0.45 nm. The hysteresis loops at relative pressure P/P_0 of 0.45–0.85 indicate the formation of mesopores. The Barret–Joyner–Halenda (BJH, Figure 1 c right) pore size distribution further revealed the mean size of mesopores to be 3 nm. The Brunauer–Emmett–Teller (BET) surface area and the total pore volume of Pd@mnc-S1 were estimated to 338 $m^2 g^{-1}$ and 0.35 cc g^{-1}, respectively, from the N_2 adsorption/desorption results. It should be noted that the contribution of voids between 200-nm-sized zeolite nanocrystals with a mean size around 30 nm was negligible here (Figure 1 c).[8] However, PVP molecules could generate more mesopores (Supporting Information, Table S1) inside the mesoporous silicalite-1 nanocrystals, further benefiting their applications as catalyst supports.

To confirm the thermal stability of encapsulated Pd nanoparticles, further calcination of as-formed Pd@mnc-S1 sample was processed at 550 °C for 6 h. A control sample with Pd nanoparticles on the surface of silicalite-1 support (Pd/silicalite-1) was also prepared and evaluated simultaneously. As shown in Figure 2 a,c, the size of Pd nanoparticles in Pd@mnc-S1 remained nearly the same before (Supporting Information, Figure S7) and after the calcination process. Such a high thermal stability confirmed that Pd nanoparticles were highly integrated inside the framework of silicalite-1 nanocrystals. Pd nanoparticles deposited on the surface of silicalite-1 support in the control sample Pd/silicalite-1 aggre-

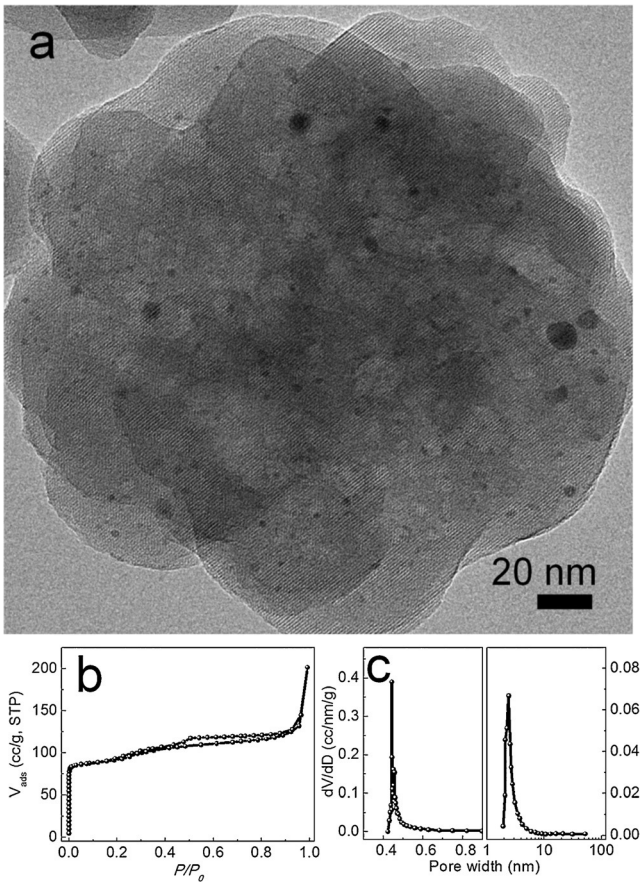

Figure 1. a) HRTEM image, b) N_2 adsorption/desorption isotherm, and c) pore size distribution of a typical Pd@mnc-S1 sample.

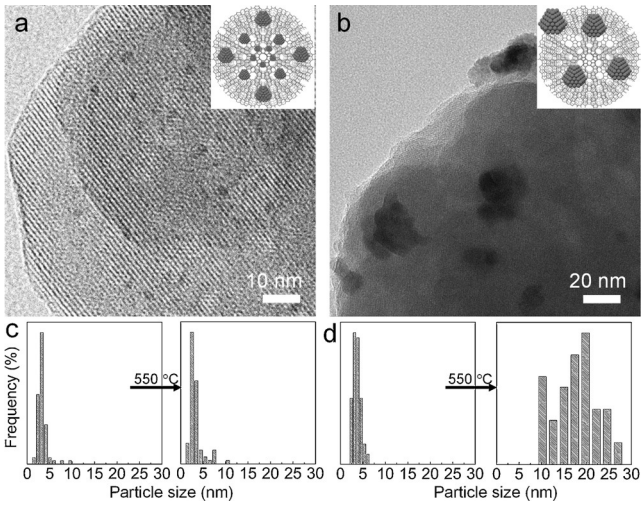

Figure 2. a),b) TEM images of a) post-treated Pd@mnc-S1 and b) the control sample Pd/silicalite-1 after calcination at 550 °C, and c),d) particle-size distribution of c) Pd@mnc-S1 and d) Pd/silicalite-1 before and after calcination.

 © 2016 Wiley-VCH Verlag GmbH & Co. KGaA, Weinheim

gated significantly (Figure 2b) with the particle size increasing dramatically from 2–5 nm to 10–30 nm after the calcination process at 550 °C (Figure 2d; Supporting Information, Figures S8, S9). Moreover, the XPS spectra (Supporting Information, Figure S10) of Pd@mnc-S1 (Pd content: 1.7 wt %) further excluded the presence of a large amount of Pd nanoparticles on the outer surface of the silicalite-1 nanocrystals. Obviously, the stabilized tiny Pd nanoparticles inside nanosized zeolites and simple synthetic strategy will benefit their potential applications as sustainable catalysts in chemical industry.

Efforts were also devoted towards evaluating the catalytic performance of Pd@mnc-S1 nanocrystals for organic synthesis as long as it is our long-term interest.[9] Hydrogenation of nitrobenzene, an important industrial reaction to produce high-value-added aniline and its derivatives, was selected as a model reaction to survey the catalytic performance of Pd@mnc-S1. As shown in Figure 3a, the hydrogenation of nitrobenzene proceeded smoothly over Pd@mnc-S1. Owing to the integrated structure of Pd@mnc-S1 with most Pd nanoparticles encapsulated inside the zeolite, the reaction rate of the catalytic conversion of nitrobenzene would be largely dominated by the mass transfer efficiency inside the micropores of MFI zeolite.[6] Surprisingly, Pd@mnc-S1 could offer a conversion of 87 % within 2 min, comparable to the conversion (98 %) over Pd/C (Supporting Information, Figure S11), on the surface of which Pd NPs deposited. A conversion of 94 % could be achieved within 5 min over Pd@mnc-S1 (Supporting Information, Tables S2–S3). The anchored Pd NPs did not obviously block the pores of silicalite-1 for possible catalytic reactions. More importantly, the mesopores and nanometer size of the zeolite nanocrystals shortened the transfer path of substrates to the Pd nanoparticles inside Pd@mnc-S1 and thus significantly accelerated the reaction rate, resulting in a catalytic activity of Pd@mnc-S1 comparable to uncovered Pd nanoparticles.

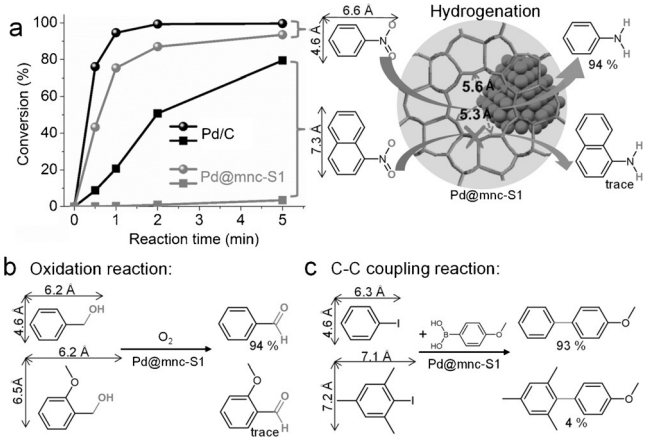

Figure 3. a) Hydrogenation reactions, b) oxidation reactions, and c) C–C coupling reactions over Pd@mnc-S1 or Pd/C. Typical conditions: i) 0.1 mmol nitrobenzene (spheres)/1-nitronaphthalene (cubes), 20 mg of Pd@mnc-S1 (gray) or 7 mg of 5 wt.% Pd/C (black), 0.2 mmol $NaBH_4$, 5 mL of H_2O, room temperature, 5 min; ii) 2 mmol of benzyl alcohol or 2-methoxybenzyl alcohol, 20 mg of Pd@mnc-S1, 20 mg of K_2CO_3, 2 mL of toluene, 1 MPa O_2, 100 °C, 3.5 h; iii) 0.2 mmol of iodobenzene/ trimethyl iodobenzene, 0.6 mmol of 4-methoxyphenylboronic acid, 20 mg of Pd@mnc-S1, 1 mmol K_2CO_3, 80 °C, 30 min. Yields of certain products were demonstrated via gas chromatography or gas chromatography–mass spectrometry analysis.

Considering the shape-selective property of zeolite support, we further tested the molecule-size dependent selectivity of Pd@mnc-S1 in the same catalytic system. For commercial Pd/C with Pd nanoparticles accessible to all molecules, the hydrogenation of most nitroarenes, independent of their molecule size, could proceed to give corresponding amines. For example, the conversion of 1-nitronaphthalene over Pd/C could reach to 80 % within 5 min, and a completely conversion could also be achieved simply by prolonging the reaction time. In contrast, only a negligible amount of 1-nitronaphthalene was converted into naphthalen-1-amine over Pd@mnc-S1, because 1-nitronaphthalene with a large molecule size (7.3 × 6.6 Å) could not pass through the micropores (pore size: 5.3 × 5.6 Å) of silicalite-1 (Figure 3a). All these results unambiguously demonstrated the shape-dependent selectivity of Pd@mnc-S1 for hydrogenation of various nitroarenes.

The shape selectivity of Pd@mnc-S1 was general for various catalytic reactions, and not limited to the hydrogenation of nitroarenes. The use of Pd@mnc-S1 was also extended to selective oxidation (Figure 3b) and C–C coupling reactions (Figure 3c). Aerobic oxidation of benzyl alcohol to benzaldehyde, which is one of the most powerful and convenient synthetic paths to produce chlorine-free benzaldehyde, was achieved over Pd@mnc-S1. For the oxidation of benzyl alcohol, benzaldehyde was the only product with a yield of 94 %. The possible byproduct, benzyl benzoate, was not detected (Supporting Information, Table S4). The shape selectivity of Pd@mnc-S1 depressed the formation of benzyl benzoate owing to the relatively larger size (12.4 × 6.3 Å) of benzyl benzoate as compared with the pore size (5.3 × 5.6 Å) of silicalite-1. As expected, the oxidation of benzyl alcohol derivatives is hindered with large molecule size, exemplified with 2-methoxylbenzyl alcohol here, could not proceed over Pd@mnc-S1, again, due to its shape selectivity (Supporting Information, Table S5). Similar shape selectivity of Pd@mnc-S1 was also observed in Pd nanoparticle-catalyzed C–C coupling reactions of iodobenzene and 4-methoxyphenylboronic acid with highly depressed yields (Figure 3c; Supporting Information, Tables S6, S7) for large-size molecules (for example 93 % for iodobenzene vs. 4 % for 2,4,6-trimethyliodobenzene). All of these results unambiguously confirmed that shape selectivity of Pd@mnc-S1 was general for a series of catalytic reactions.

Furthermore, the reusability of Pd@mnc-S1, as an important issue of heterogeneous catalysts for practical use at large scales, was also studied here. Taking the C–C coupling reaction as an example, commercial Pd/C was widely used as the catalyst to construct unsymmetrical biaryl compounds in fine chemistry. The poor stability of Pd/C significantly elevated the final price of corresponding products.[10] Recycling uses of Pd@mnc-S1 was carried out here simply by separating the used catalyst from the mother solution of the first reaction via centrifugation and directly used for the next run under fixed conditions. As shown in Figure 4, Pd@mnc-S1 remained highly active, with the yield of 4-methoxy biphenyl

 © 2016 Wiley-VCH Verlag GmbH & Co. KGaA, Weinheim

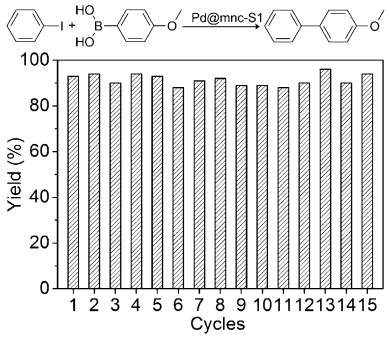

Figure 4. Multiple uses of the Pd@mnc-S1 catalyst for the C–C coupling reaction. Typical conditions are described in Figure 3.

maintained at around 93% during the following 15 cycles of reactions. TEM observations (Supporting Information, Figure S12) further demonstrated that the size and distribution of Pd nanoparticles remained nearly the same after 15 cycles of reactions. Obvious Pd leaching during the reaction was also excluded here according to the inductively coupled plasma (ICP) result (data not shown), with the concentration of leached Pd species in the reaction solution below the detection limit of the equipment. The well-established reusability of Pd@mnc-S1 could obviously benefit its practical applications in the future.

In summary, we have successfully constructed highly integrated Pd/zeolite hybrids with Pd nanoparticles encapsulated inside mesoporous silicalite-1 nanocrystals. The as-synthesized Pd@mnc-S1 showed high stability and general shape-selectivity owing to its unique nanostructure and porosity. The mesoporous structure as well as the nanosized crystals of the catalyst support were preferred for promoting mass transfer to Pd nanoparticles and their final catalytic performance. Our synthetic strategy increases the scope of on-demand controlling the selectivity of metal nanoparticles by rationally selecting zeolite support mainly on the basis of their pore size without significantly sacrificing the catalytic activity of the metal nanoparticle/zeolite dyads.

Acknowledgements

This work was financially supported by the National Basic Research Program of China (2013CB934102), the National Natural Science Foundation of China (21331004, 21301116), and Shanghai Eastern Scholar Program.

Keywords: mesoporous materials · nanocrystals · palladium · shape-selective catalysis · zeolites

How to cite: *Angew. Chem. Int. Ed.* **2016**, *55*, 9178–9182
Angew. Chem. **2016**, *128*, 9324–9328

[1] a) Y.-Y. Cai, X.-H. Li, Y.-N. Zhang, X. Wei, K.-X. Wang, J.-S. Chen, *Angew. Chem. Int. Ed.* **2013**, *52*, 11822–11825; *Angew. Chem.* **2013**, *125*, 12038–12041; b) L.-T. Guo, Y.-Y. Cai, J.-M. Ge, Y.-N. Zhang, L.-H. Gong, X.-H. Li, K.-X. Wang, Q.-Z. Ren, J. Su, J.-S. Chen, *ACS Catal.* **2015**, *5*, 388–392; c) L.-H. Gong, Y.-Y. Cai, X.-H. Li, Y.-N. Zhang, J. Su, J.-S. Chen, *Green Chem.* **2014**, *16*, 3746–3751.

[2] a) Q. Yue, Y. Zhang, C. Wang, X. Wang, Z. Sun, X.-F. Hou, D. Zhao, Y. Deng, *J. Mater. Chem. A* **2015**, *3*, 4586–4594; b) Q.-L. Zhu, J. Li, Q. Xu, *J. Am. Chem. Soc.* **2013**, *135*, 10210–10213; c) G. Li, H. Kobayashi, J. M. Taylor, R. Ikeda, Y. Kubota, K. Kato, M. Takata, T. Yamamoto, S. Toh, S. Matsumura, H. Kitagawa, *Nat. Mater.* **2014**, *13*, 802–806; d) W. Li, D. Zhao, *Adv. Mater.* **2013**, *25*, 142–149; e) P. M. Arnal, M. Comotti, F. Schüth, *Angew. Chem. Int. Ed.* **2006**, *45*, 8224–8227; *Angew. Chem.* **2006**, *118*, 8404–8407; f) H. Zhu, C. Liang, W. Yan, S. H. Overbury, S. Dai, *J. Phys. Chem. B* **2006**, *110*, 10842–10848; g) B. Li, B. Sun, X. Qian, W. Li, Z. Wu, Z. Sun, M. Qiao, M. Duke, D. Zhao, *J. Am. Chem. Soc.* **2013**, *135*, 1181–1184; h) J. Gu, Z. Zhang, P. Hu, L. Ding, N. Xue, L. Peng, X. Guo, M. Lin, W. Ding, *ACS Catal.* **2015**, *5*, 6893–6901.

[3] a) P. M. Arnal, C. Weidenthaler, F. Schüth, *Chem. Mater.* **2006**, *18*, 2733–2739; b) K. Bakhmutsky, N. L. Wieder, M. Cargnello, B. Galloway, P. Fornasiero, R. J. Gorte, *ChemSusChem* **2012**, *5*, 140–148.

[4] a) X.-H. Li, X. Wang, M. Antonietti, *Chem. Sci.* **2012**, *3*, 2170–2174; b) Z. Wu, Y. Lv, Y. Xia, P. A. Webley, D. Zhao, *J. Am. Chem. Soc.* **2012**, *134*, 2236–2245; c) R. Liu, S. M. Mahurin, C. Li, R. R. Unocic, J. C. Idrobo, H. Gao, S. J. Pennycook, S. Dai, *Angew. Chem. Int. Ed.* **2011**, *50*, 6799–6802; *Angew. Chem.* **2011**, *123*, 6931–6934; d) D. Shen, L. Chen, J. Yang, R. Zhang, Y. Wei, X. Li, W. Li, Z. Sun, H. Zhu, A. M. Abdullah, A. Al-Enizi, A. A. Elzatahry, F. Zhang, D. Zhao, *ACS Appl. Mater. Interfaces* **2015**, *7*, 17450–17459; e) T. Ge, Z. Hua, X. He, J. Lv, H. Chen, L. Zhang, H. Yao, Z. Liu, C. Lin, J. Shi, *Chem. Eur. J.* **2016**, *22*, 7895–7905; f) W. Wang, G. Li, W. Li, L. Liu, *Chem. Commun.* **2011**, *47*, 3529–3531; g) C. Dai, A. Zhang, M. Liu, X. Guo, C. Song, *Adv. Funct. Mater.* **2015**, *25*, 7479–7487.

[5] a) Q. Fang, S. Gu, J. Zheng, Z. Zhuang, S. Qiu, Y. Yan, *Angew. Chem. Int. Ed.* **2014**, *53*, 2878–2882; *Angew. Chem.* **2014**, *126*, 2922–2926; b) S. H. Pang, C. A. Schoenbaum, D. K. Schwartz, J. W. Medlin, *Nat. Commun.* **2013**, *4*, 2448; c) M. Sadakiyo, T. Yamada, K. Kato, M. Takata, H. Kitagawa, *Chem. Sci.* **2016**, *7*, 1349–1356; d) C. P. Canlas, J. Lu, N. A. Ray, N. A. Grosso-Giordano, S. Lee, J. W. Elam, R. E. Winans, R. P. Van Duyne, P. C. Stair, J. M. Notestein, *Nat. Chem.* **2012**, *4*, 1030–1036.

[6] a) J. Mielby, J. O. Abildstrøm, F. Wang, T. Kasama, C. Weidenthaler, S. Kegnæs, *Angew. Chem. Int. Ed.* **2014**, *53*, 12513–12516; *Angew. Chem.* **2014**, *126*, 12721–12724; b) A. B. Laursen, K. T. Hoejholt, L. F. Lundegaard, S. B. Simonsen, S. Helveg, F. Schueth, M. Paul, J.-D. Grunwaldt, S. Kegnaes, C. H. Christensen, K. Egeblad, *Angew. Chem. Int. Ed.* **2010**, *49*, 3504–3507; *Angew. Chem.* **2010**, *122*, 3582–3585; c) N. Ren, Y.-H. Yang, Y.-H. Zhang, Q.-R. Wang, Y. Tang, *J. Catal.* **2007**, *246*, 215–222; d) N. Ren, Y.-H. Yang, J. Shen, Y.-H. Zhang, H.-L. Xu, Z. Gao, Y. Tang, *J. Catal.* **2007**, *251*, 182–188; e) S. Li, T. Boucheron, A. Tuel, D. Farrusseng, F. Meunier, *Chem. Commun.* **2014**, *50*, 1824–1826; f) S. Li, C. Aquino, L. Gueudré, A. Tuel, Y. Schuurman, D. Farrusseng, *ACS Catal.* **2014**, *4*, 4299–4303; g) C. Dai, X. Li, A. Zhang, C. Liu, C. Song, X. Guo, *RSC Adv.* **2015**, *5*, 40297–40302.

[7] a) L.-H. Chen, X.-Y. Li, J. C. Rooke, Y.-H. Zhang, X.-Y. Yang, Y. Tang, F.-S. Xiao, B.-L. Su, *J. Mater. Chem.* **2012**, *22*, 17381–17403; b) D. P. Serrano, J. M. Escola, P. Pizarro, *Chem. Soc. Rev.* **2013**, *42*, 4004–4035.

[8] T.-L. Cui, X.-H. Li, L.-B. Lv, K.-X. Wang, J. Su, J.-S. Chen, *Chem. Commun.* **2015**, *51*, 12563–12566.

[9] a) Y. Tian, G.-D. Li, J.-S. Chen, *J. Am. Chem. Soc.* **2003**, *125*, 6622–6623; b) L. Li, X.-S. Zhou, G.-D. Li, X.-L. Pan, J.-S. Chen, *Angew. Chem. Int. Ed.* **2009**, *48*, 6678–6682; *Angew. Chem.* **2009**, *121*, 6806–6810; c) L. Li, G. D. Li, C. Yan, X. Y. Mu, X. L. Pan, X. X. Zou, K. X. Wang, J. S. Chen, *Angew. Chem. Int. Ed.*

 © 2016 Wiley-VCH Verlag GmbH & Co. KGaA, Weinheim

2011, *50*, 8299 – 8303; *Angew. Chem.* **2011**, *123*, 8449 – 8453; d) L. Li, Y. Y. Cai, G. D. Li, X. Y. Mu, K. X. Wang, J. S. Chen, *Angew. Chem. Int. Ed.* **2012**, *51*, 4702 – 4706; *Angew. Chem.* **2012**, *124*, 4780 – 4784; e) X.-H. Li, M. Baar, S. Blechert, M. Antonietti, *Sci. Rep.* **2013**, *3*, 1743; f) X.-H. Li, Y.-Y. Cai, L.-H. Gong, W. Fu, K.-X. Wang, H.-L. Bao, X. Wei, J.-S. Chen, *Chem. Eur. J.* **2014**, *20*, 16732 – 16737; g) J.-F. Wang, K.-X. Wang, J.-Q. Wang, L. Li, J.-S. Chen, *Chem. Commun.* **2012**, *48*, 2325 – 2327.

[10] a) A. Fihri, M. Bouhrara, B. Nekoueishahraki, J.-M. Basset, V. Polshettiwar, *Chem. Soc. Rev.* **2011**, *40*, 5181 – 5203; b) L. Shao, B. Zhang, W. Zhang, S. Y. Hong, R. Schlögl, D. S. Su, *Angew. Chem. Int. Ed.* **2013**, *52*, 2114 – 2117; *Angew. Chem.* **2013**, *125*, 2168 – 2171.

Received: March 9, 2016
Revised: May 18, 2016
Published online: June 27, 2016

 © 2016 Wiley-VCH Verlag GmbH & Co. KGaA, Weinheim